Simulation of lithium distribution and diffusion pathways in Li_6PS_5X (X = Cl, Br, I) and Li_7PX_6 (X = S, Se) by means of ab-initio molecular dynamics

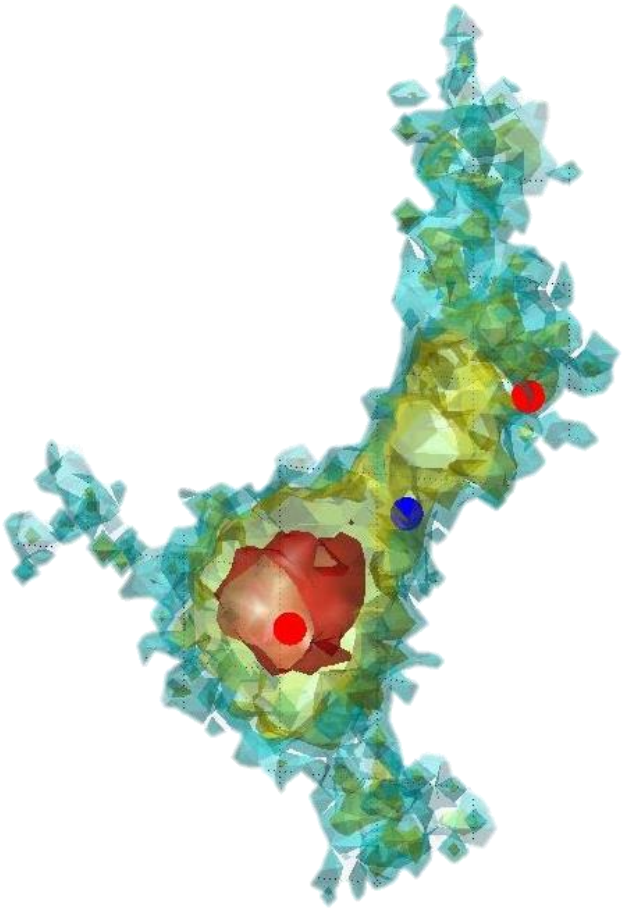

Bachelor thesis
By I.E. Rosłoń
To be defended on March 21st 2016

Reactor Institute Delft
Fundamental Aspects of Material and Energy group
Faculty of Applied Science
Delft University of Technology

Supervisor: dr. ir. M. Wagemaker
Second examiner: dr. ir. A. van Well

Abstract

Diffusivities and lithium distributions in Li_6PS_5X (X = Cl, Br, I) and Li_7PX_6 (X = S, Se) are investigated by means of molecular dynamics simulations. The best lithium conduction is found in Li_6PS_5Cl with diffusivity of over 1 S/cm at 600 K. The halide rich $Li_5PS_4Cl_2$ shows promising results with diffusivity of over 2 S/cm at 600 K, performing better in simulations than the existing compounds.

Simulations show a beneficent effect of chlorine and bromine disorder on anion sites, opening lithium pathways in the neighborhood and enabling higher conductivities. No significant influence of vacancies on the diffusivity of lithium in these materials can be reported. Lithium jump rates in both material families are in the order of 10^{10} s^{-1}, while Li_6PS_5Cl and $Li_5PS_4Cl_2$ show the highest jump rates of respectively $2.10 \cdot 10^{11}$ s^{-1} and $2.14 \cdot 10^{11}$ s^{-1} at 600 K.

Table of contents

Symbols and abbreviations

Table 1 List of symbols in order of appearance

Symbol	Quantity	Unit	Unit in words
D	Diffusivity	m^2s^{-1}	Square meter per second
J	Flux	$t^{-1}m^{-2}$	Mole per square meter per second
φ	Concentration	m^{-3}	Mole per cubic meter
x	Distance	m	Meter
Γ	Jump rate	s^{-1}	Per second
n	Number	-	-
λ	Jump distance	m	Meter
V	Volume	m^3	Cubic meters
f	Frequency	s^{-1}	Per second
m	Mass	kg	Kilogram
v	Velocity	ms^{-1}	Meter per second
t	Time	s	Second
F	Force	N	Newton
d	Number of dimensions	-	-
$\vec{r}$	Place vector	m	Meter
C	Conductivity	S/cm	Siemens per centimeter
R	Universal gas constant	$JK^{-1}mol^{-1}$	Joule per Kelvin per mole
F_C	Faraday's constant	$Cmol^{-1}$	Coulomb per mole
z	Ionic charge	C	Coulomb
T	Temperature	K	Kelvin
c_v	Coefficient of variation	-	-
σ	Standard deviation	-	-
μ	Mean	-	-

Table 2 List of abbreviations in order of appearance

Abbreviation	Meaning
VASP	Vienna Ab-Initio Simulation Package
DFT	Density Functional Theory
PAW	Projector Augmented Wave method
MSD	Mean Square Displacement
MD	Molecular Dynamics
GGA	Generalized Gradient Approximation
PBE	Perdew-Burke-Ernzerhof

Introduction

Batteries are one of the most frequently used devices in everyday life, especially in products that require high portability or have low accessibility. These batteries are often a limiting factor in product performance, causing consumers to desire batteries to become lighter, to last longer and to be safer. Profound understanding of the physics behind them is a key to manufacturing even better ones. A promising research field concerning batteries is that of all solid batteries. The aim of this research is to gain deeper understanding of solid state electrolytes and improve battery characteristics.

A simple battery consists of two electrodes where chemical reactions generate electrical energy. As electrons flow from one electrode to another through an external circuit, ions have to pass through an electrolyte to keep a steady-state charge distribution in the battery. Lithium frequently acts as ionic conductor and batteries of this type are depicted Li-ion batteries; their use is widely spread in consumer products such as mobile cell phones and electric vehicles.

Because an electrolyte is a passageway for ions, connecting the electrodes, it has to be both an electric insulator and a good ionic conductor. Frequently used electrolytes are liquids that show high ionic conductivity. (1) They have to be packed well to prevent leakage and give protection against their high flammability. Solid state electrolytes need less packaging since they cannot leak and have increased mechanical and thermal stability compared to liquids. (2) On the other hand, solids are by their nature far less favorable in achieving high ionic conductivities.

Materials from both the Li_6PS_5X (X = Cl, Br, I) and Li_7PX_6 (X = S, Se) families are reported to be promising for use as solid state electrolytes. (3) These materials are electric insulators and have shown high lithium ion conductivities in practice. (4) Goal of this research is to broaden the understanding of Lithium transport in these argyrodite type crystals by means of molecular dynamics simulations and find ways of improving their performance.

Theory

The crystal structure adopted by a particular material depends on the nature of the forces between the atoms within it. In some materials, particularly metals, a good approximation is that of attracting hard spheres packed closely together. (5) The argyrodite type materials cannot be described this way because of the far bigger spacing in their structures, that is allowing even for macroscopic diffusivity in some cases. Because of the complexity of the structures a far more elaborate approximation is needed, which is implemented in the Vienna Ab-Initio Simulation Package (VASP).

Ab-Initio Molecular Dynamics

The exact movement of molecules in a material can be simulated using a computer. Solutions to Newton's equations of motion for many body problems are numerically approximated based on the potentials obtained from electronic structure calculations of the atoms involved. The Ab-Initio part refers to the on-the-fly calculations of the electronic structures, highly improving the results compared to methods neglecting electronic degrees of freedom.

With Density Functional Theory (DFT) the Schrodinger equation can be simplified into one with less variables. Rather than adding each electron separately, one uses the electron density and performs calculations with functionals (functions with a function as input instead of a variable). (6) Also, several approximations are used in order to speed up the calculations; the most important ones are listed below.

Pseudopotentials

The effective potential of an atom is mainly depending on electrons in the outer shell, the valence electrons. (5) Therefore the complicated interactions between the nucleus and the inner electrons can be replaced by a less complicated pseudopotential and corresponding wave function. Since this replacement is not valid for short distances, a cut-off radius or energy has to be specified.

Projector Augmented Wave method

The pseudopotentials have characteristic shapes and symmetries, allowing for easier description than with a set of plane waves. The Projector Augmented Wave method (PAW) incorporates these simplifications into DFT allowing for more efficient calculations. (7) Essentially, the fact that the electron density is expected to be smooth is exploited to find regions of constant density.

Hopping and jump frequency

This study primarily considers the diffusion of lithium through crystals. All crystals reported in this thesis share the same crystallographic properties of the cubic *F*-43*m* space group. This implies symmetries on the crystal lattice leading to a characteristic ordering of all atoms; the spots possibly occupied by lithium are the 24g and 48h sites. (3)

Although lithium has fixed crystallographic sites it most likely resides on, it still is highly mobile in the studied materials. The high mobility implies that lithium is able to move between crystallographic sites. In general one can say that lithium migration trough a solid is the result of a sequence of jumps from one site to another. (8) When looking at an arbitrary plane in a crystal, the difference in hops forward and backward trough that plane equals the net flux *J*. Identifying the concentration φ as number of atoms per jump distance λ, and combining this with Fick's law yields an expression for the diffusivity *D* of the Li atoms:

$$D = -\frac{J}{\left(\frac{\partial \varphi}{\partial x}\right)} = \frac{\Gamma*(n_1 - n_2)}{\left(\frac{n_1 - n_2}{\lambda^2}\right)} = \Gamma * \lambda^2 \qquad (1)$$

Where Γ is the jump rate trough the plane and *n* stands for the number of atoms on each side of the plane. The derivative of φ is approximated to first order by the difference in *n* over a distance λ. A jump event is therefore identified as a displacement from one crystal site to another.

Delaunay triangulation

The Delaunay triangulation is an algorithm allowing for fast geometric nearest neighbor searches. It allows to find nearest neighbors and distances by matrix multiplication and determinant evaluation, which both can be quickly done with a computer. This features are used for finding lithium sites and occupancies.

Debye frequency

The Debye frequency is a theoretical maximum frequency of thermal vibration for atoms in a crystal. (5) Generally this frequency is an upper limit to the actual thermal vibrations in a crystal. The Debye frequency f_D is given by the number density of atoms n/*V* and the effective speed of sound v_s:

$$f_D = \left(\frac{3n}{4\pi V}\right)^{1/3} v_s \qquad (2)$$

In order to distinguish crystal vibrations from hopping during the simulations, it is required that an atom resides at another crystal site for at least more than one thermal vibration to count as a hop. For the crystals simulated the Debye frequency is in the order of 10^{12} s^{-1}, based on *n = 56* in a cubic lattice with length 10 Angstrom and a speed of sound of approximately 10^3 m/s.

Brownian motion

The movements of the Li atoms can also be analyzed as if they were particles performing a random walk. External forces are propelling this particle through the crystal. Also, the particle is being hold back by a 'friction' force due to its surroundings. When these forces are in equilibrium, the whole system will reach a steady state and the particle will flow at a steady average velocity. For a moving particle the equation of motion reads (9):

$$m\frac{d\vec{v}}{dt} = \sum \vec{F} \tag{3}$$

A second step takes into account the randomness of the motion of a particle performing a random walk and leads to the Langevin equation. The particle is modelled to bump up and down, forwards and backwards, in a totally random way. It is called to execute a Brownian motion. Adding the random force *R(t)* to the previous equation gives the Langevin equation:

$$m\frac{d\vec{v}}{dt} = \sum \vec{F} + \vec{R}(t) \tag{4}$$

Diffusivity

Brownian motion is the random movement of particles performing a random walk, a process which is quantified by the diffusivity *D*. In essence this value tells you how much a particle moves in a certain time. Therefore the diffusivity *D* is proportional to the Mean Square Displacement (MSD) of the atoms involved; (10) Nernst and Einstein have first derived this from the Langevin equation:

$$D = \frac{1}{2d}\lim_{t\to\infty}\frac{\langle[\vec{r}(t_0+t)-\vec{r}(t_0)]^2\rangle}{t} \approx \frac{MSD}{6t} \tag{5}$$

Here *d* is the number of dimensions in which the process happens (in this case three) and *t* is the time elapsed during the diffusion process. The MSD is defined as the ensemble average of the squared displacements *r* during a process. It is evident that simulation times cannot go to infinity, but have to be chosen sufficiently long for realistic approximations.

Conductivity

The ionic conductivity *C* of a material expresses the ability of conducting ions trough a material. (9) When the ions are treated as if they were particles with charge *z*, the conductivity can be related to the diffusivity by the physical constants *R* and F_c, and the temperature *T*:

$$C = D * \frac{(F_c * z)^2}{R * T} \quad (6)$$

Coefficient of variation

The coefficient of variation c_v is a statistical tool allowing for comparison of standard deviations. This coefficient is a scaled standard deviation defined by the following formula:

$$c_v = \frac{\sigma}{\mu} \quad (7)$$

With μ the mean of a dataset and σ the corresponding standard deviation.

Methodology

Based on ab-initio Molecular Dynamics (MD) simulations the trajectories of the atoms within the crystal are simulated. The Vienna Ab Initio Simulation Package (in short VASP) is used for this task. It approximates solutions to the many-body Schrodinger equation with Density Functional Theory (DFT). The DFT MD-simulations were performed using the GGA approach, with the PAW-PBE basis set as implemented in VASP. (11) A single unit cell was used, for the minimizations a k-point mesh of 2x2x2, and for the MD-simulations a k-point mesh of 1x1x1. In total a time of 100 picoseconds was simulated, with time-steps of 2 femtoseconds.

Raw trajectory data of all atoms in the MD simulations from VASP are processed by Matlab and Fortran routines. The time allowed for equilibration was 2.5 picoseconds in the Fortran routines and 10 picoseconds in the Matlab routines. Whenever possible without information loss data are sampled during jump frequency calculations for faster computation. Stability of MD-simulations is verified by all-atom MSD plots and crystallographic site displacement comparison with initial values. Conductivities and diffusivities are calculated based on both Li-MSD and Li-jump frequencies, using varying equilibration times.

Identification of crystallographic site occupation is performed using a Delaunay triangulation of an extended unit cell. Also, jumps events are identified and times of residence are calculated. The jumps include irrelevant random thermal movement, which is characterised by short times of residence in the order of the Debye frequency. A low pass filter on the jump frequency is used to remove this thermal noise. The jump filter is limited to there and back again events and the filter settings are based on the Debye criterion. Density maps are made by binning the trajectories into cubes with edge length of 0.1 Angstrom. Colours are associated with a quadratic density mapping.

Materials simulated

Two existing families of structures, Li_6PS_5X (X = Cl, Br, I) and Li_7PX_6 (X = S, Se), are simulated and analyzed using the methods mentioned above. For comparative analysis on the influence of lithium vacancies theoretical study on Li_nPS_5Cl (n = 5, 7) and Li_6PS_6 is performed. On account of promising intermediate results, also a $Li_5PS_4Cl_2$ and a Li_6PS_5Ar structure have been simulated.

Results

Simulations are performed for several crystals using VASP. Three simulations are performed for each material at 300, 450 and 600 Kelvin. Table 3 lists all materials simulated with their Li-conductivities at 600 Kelvin based on the respective MSD's.

Table 3 List of all simulated materials and their conductivities at 600 K.

	Material structure	Conductivity at 600 K (S/cm)
Existing compounds	Li_7PS_6	0.438
	Li_6PS_5Cl	1.01
	Li_6PS_5Cl (2x1x1 supercell)	0.840
	Li_6PS_5Br	0.845
	Li_6PS_5I	0.080
	Li_7PSe_6	0.730
Theoretical compounds	Li_6PS_6	0.443
	Li_7PS_5Cl	0.180[1]
	Li_5PS_5Cl	0.370[2]
	$Li_5PS_4Cl_2$	2.04
	Li_6PS_5Ar	-[3]

In order to validate the consistency and spread of the results multiple runs with the same starting conditions are performed for Li_7PS_6. This compound is chosen because it is best described in literature and by experimental studies. (12) With rising temperature the spread in the results becomes smaller, since the actual value for diffusivity should be better approximated with increased jumping activity. As listed in Table 4, within four runs at 300 Kelvin the coefficient of variation for the mean square displacement equals 0.33, whilst at 600 Kelvin the same coefficient equals 0.08.

Table 4 Coefficients of variation for the mean square displacement of diffusing lithium over 4 MD simulations of Li_7PS_6 at varying temperatures. The coefficient of variation is lower at higher temperatures because of the higher diffusivity.

Temperature (K)	Mean conductivity (S/cm)	Coefficient of variation (-)
300	0.054	0.33
450	0.30	0.22
600	0.50	0.08

[1] Unstable at 600 K, results listed for 450 K.
[2] Unstable at 600 K, results listed for 450 K.
[3] No data available because of structure instability.

Exact calculation of the variation for each material requires multiple runs with the same starting conditions. This approach is highly ineffective and computational power is limited. Therefore other materials are assumed to have comparable coefficients of variation. The assumption is reasonable, since the crystals are much alike and the temperature dependence of the diffusivity is expected and found in all simulated compounds. Even if calculated, errors bars are left away to make the figures more clear. In the next chapters the conductivity data, jump rates and Li-pathways are thoroughly discussed for all compounds.

Conductivity data

Figure 1 shows conductivities calculated from the Li MSD's. Comparison of conductivity data shows that Li_6PS_5Cl is the best Li conductor from the Li_7PX_6 (X = S, Se) and Li_6PS_5X (X = Cl, Br, I) families, with a conductivity of over 1 S/cm at 600 K, while the Li_6PS_5I compound performs significantly worse from the others. The data points of Li_7PS_6 show the spread in the results. It should also be mentioned that in consequence of the low activity and limited simulation time the spread in the results at 300K is very large, resulting in much overlap between the data points and low reliability.

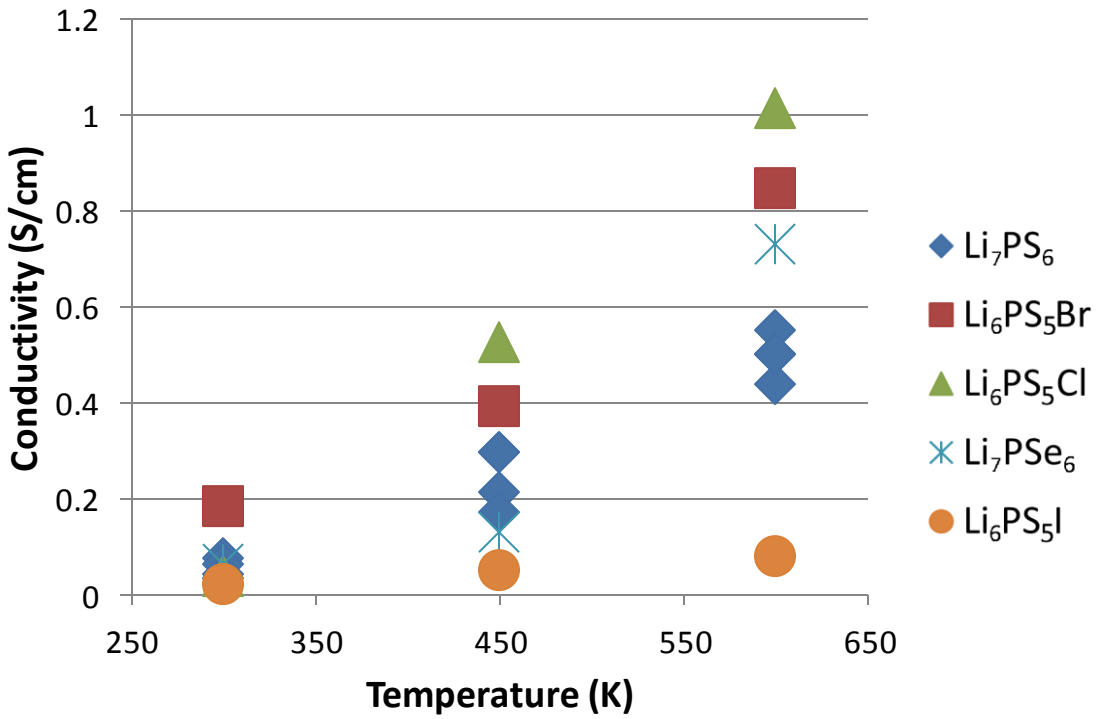

Figure 1 Conductivities in Li_7PX_6 (X = S, Se) and Li6PS5X (X = Cl, Br, I) based on Li MSD's. Clearly, Li_6PS_5Cl performs best and Li_6PS_5I performs significantly worse compared to all the other materials.

Next to the two existing families of materials, several theoretical materials are simulated for comparison and analysis purposes. The $Li_5PS_4Cl_2$ was stable at all temperatures, and showed promising results with a conductivity of over 2 S/cm at 600 K. Two other materials simulated, Li_nPS_5Cl (n = 5, 7), suffered from instability at an elevated temperature of 600 K, whereas Li_6PS_5Ar was not stable at all. Figure 2 shows conductivities for all stable theoretical materials simulated.

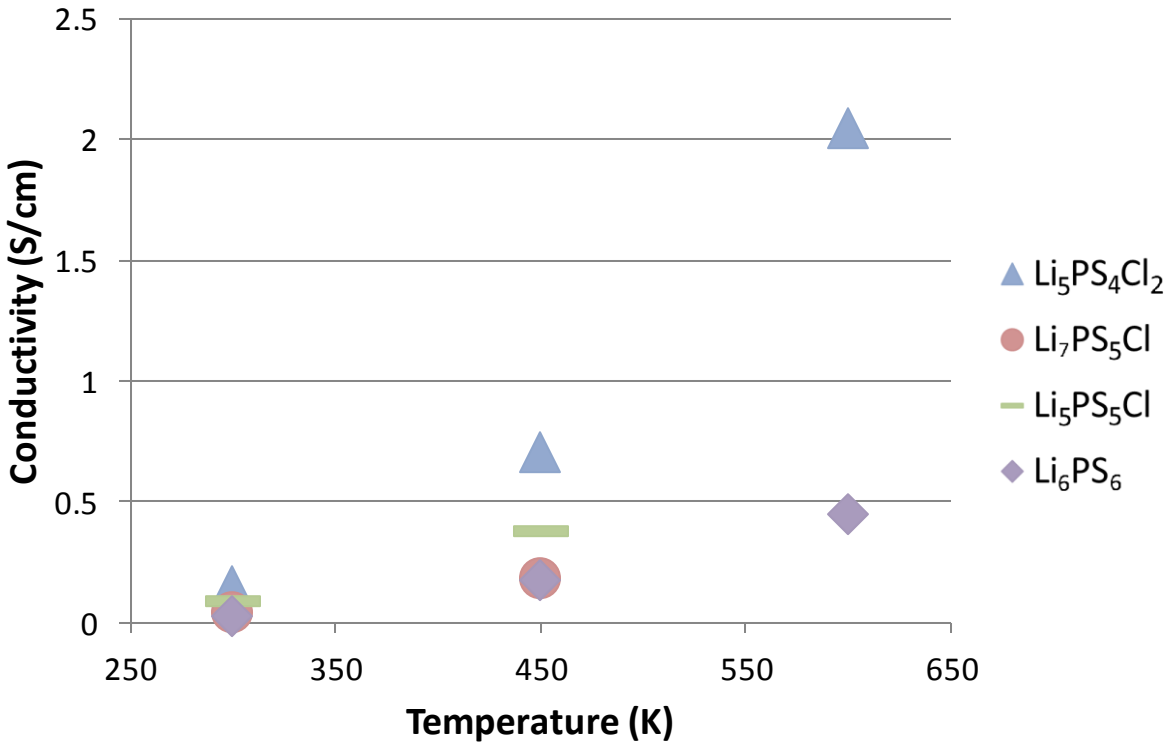

Figure 2 Conductivities in Li_nPS_5Cl (n = 5, 7), $Li_5PS_4Cl_2$ and Li_6PS_6 based on Li MSD's. Note that the data points of Li_5PS_5Cl and Li_6PS_6 overlap slightly. Clearly $Li_5PS_4Cl_2$ outperforms all other materials as to conductivity.

Pathway categorization

Based on the molecular dynamics data density plots are made for all the materials. Since they belong to the same space group, the diffusion pathways are similar in all simulations. These pathways can be divided into 3 categories, mainly depending on the distance between the crystallographic sites occupied, as indicated in Table 5. (13) The categorization is used to investigate the Li-pathways and jump frequencies in a structured manner.

Table 5 Pathway categorization and typical values for jump distance and energy barrier

Pathway category	Characteristic description	Typical jump distance (Å)	Typical energy barrier (eV)
1	Triplet site	<2	<0.1
2	Pathway cage	2 – 3	>0.1
3	Enabling macroscopic diffusion	>3	>0.2

Triplet site (48h – 24g – 48h)

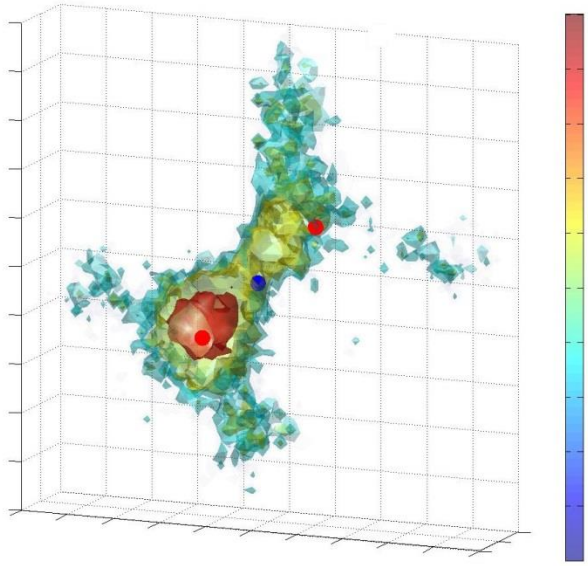

Figure 3 A triplet site in Li_6PS_5Br in a density plot at 450 Kelvin, where red stands for high occupancy and blue for low occupancy. The triplet sites consist of two red marked 48h sites with a blue marked 24g site in between. During this simulation the bottom 48h site is particularly longer occupied than the top one.

The first category with the lowest energy barrier is that between two closest pairs of 48h sites. In the halide containing materials an interstitial 24g site in between eases this passage, together forming a triplet. As a result of the very short distance between these

sites, the lithium in a crystal distributes evenly over all triplets, avoiding states in which one triplet has two Li's and another triplet is empty. This however is a necessary stadium for diffusion trough Li_6PS_5X.

Pathway cage

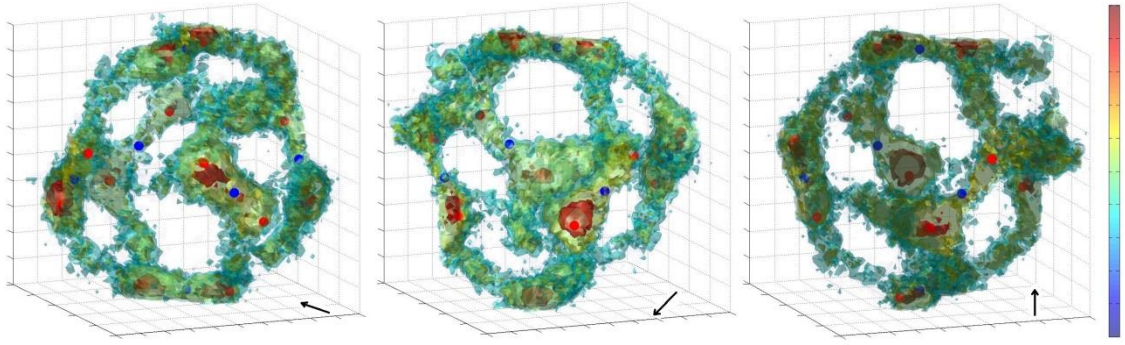

Figure 4 A single 'cage' around a bromide atom in Li_6PS_5Br as seen from different view angles in a density plot at 450 Kelvin, where red stands for high an occupancy and blue for low occupancy. The triplet sites are clearly interconnected by second category pathways forming a cage.

The second category of pathways are the links connecting the doublets and triplets into 'cages' around a halide or sulfur atom. The energy barriers between these sites are comparable or higher to those between the doublet and triplet sites. The second category pathways form on their own pathway triangles. In Li_7PX_6 materials one pathway cage comprises six doublets, that give room to seven lithium. Here, the pathway triangles are especially often occupied by the extra seventh lithium.

Cage interconnections

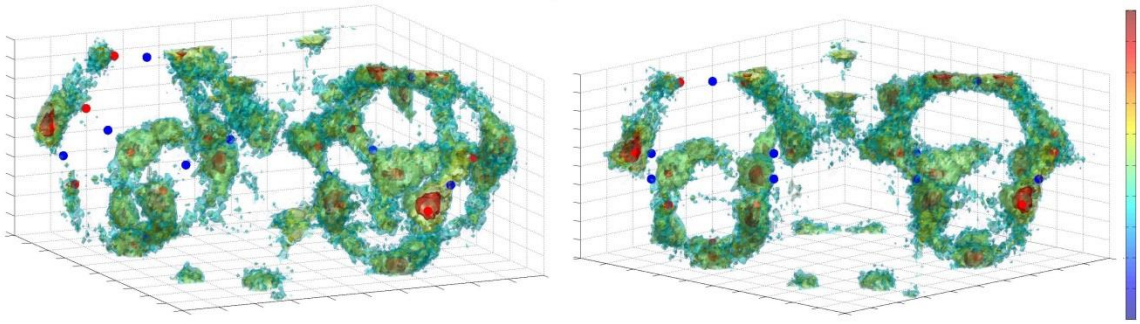

Figure 5 Two pathway cages seen from different perspectives. The connections between cages form the third category pathways.

The third category pathways are the connections between the four ‘cages’ within a unit cell. The energy barrier for these connections is the highest from the three categories. These connections are necessary for long range diffusivity of lithium through F-43m crystals. Because of their high energy barrier, they are the least likely to occur and are the main limiting factor for lithium diffusivity in these crystals.

Li_6PS_5X (X = Cl, Br, I) compounds results

The diffusion pathways have been made visible for Li_6PS_5X structures. First of all several density plots are made, that show where the lithium resides most frequently. The spots with highest density coincide with the experimental values for the crystal structure, supporting the correctness of the simulations. (13)

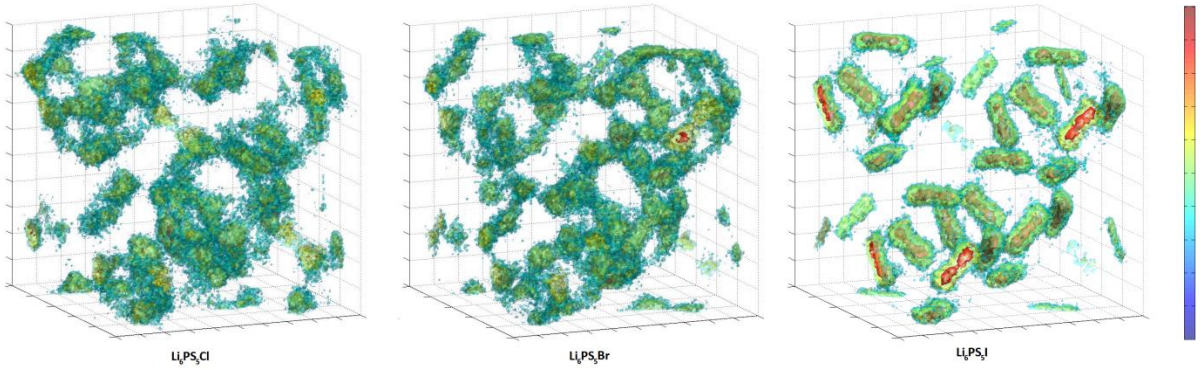

Figure 6 Li-density maps for Li_6PS_5Cl, Li_6PS_5Br and Li_6PS_5I at 600K. The Li_6PS_5Br and Li_6PS_5Cl are much alike, but Li_6PS_5I has a more localized lithium distribution.

Figure 6 shows the density plots for Li_6PS_5Cl, Li_6PS_5Br and Li_6PS_5I. Four 'cages' around the halide and sulfur atoms are clearly visible. It is also immediately visible that in the Li_6PS_5I compound, the lithium rarely moves from cage to cage, accounting for far worse conductivity compared to the other two compounds. Connections in a single cage are also far less pronounced in Li_6PS_5I.

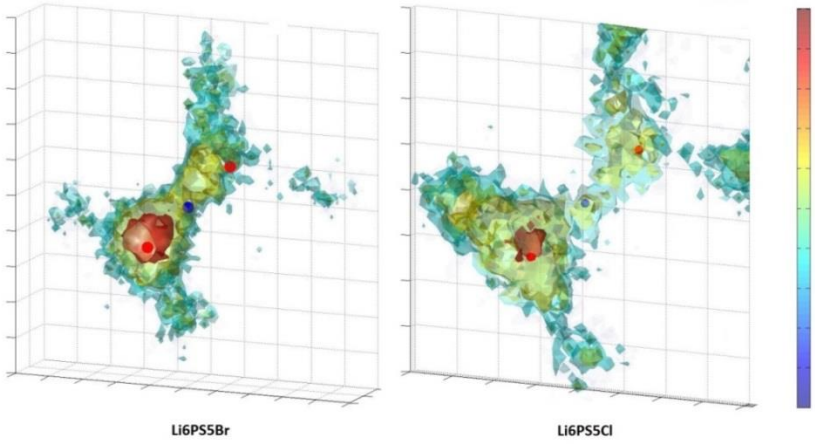

Figure 7 A triplet site in both Li_6PS_5Br (left) and Li_6PS_5Cl (right) in a density plot at 450 Kelvin, where red stands for high occupancy and blue for low occupancy. A triplet site consist of two red marked 48h sites with a blue marked 24g site in between.

A 48h-24g-48h triplet site in both Li_6PS_5Br and Li_6PS_5Cl are shown in Figure 7, with the two 48h sites marked by red dots and the interstitial 24g sites marked by blue dots. Although all three sites are well connected forming a passageway, lithium succeeds relatively rarely in jumping through. This is shown in Figure 8, where the dark blue and green color clearly mark the two 48h positions of a triplet site within a Li-trajectory during a full simulation. Seemingly the lithium moves very often over and back again, but in detail only two successful jumps occur during this simulation.

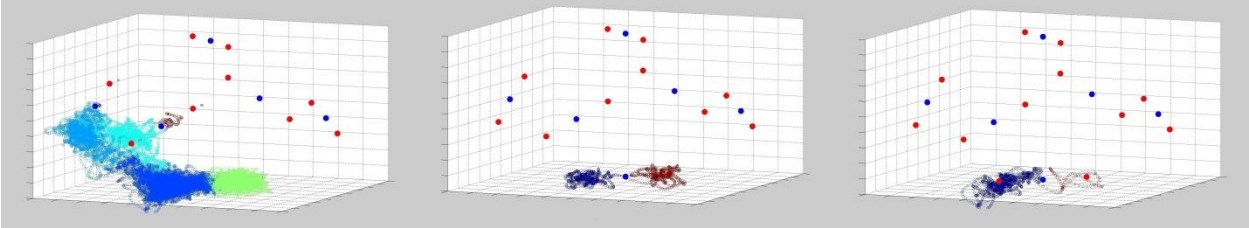

Figure 8 Trajectory of a lithium atom through Li_6PS_5Br in a MD simulation at 450 K (left). The red dots indicate 48h sites and the blue dots 24g sites. Lithium performs a total of two successful jumps through a 48h-24g-48h triplet between the regions indicated by green and dark blue. The partial trajectories during these jumps are also shown (middle and right).

To verify the simulations the lithium sites are compared to the actual crystallographic sites. During the limited timespan of simulations not all available crystallographic sites are occupied for an adequate time at 300 K and 450 K, sometimes resulting in extreme variations. This does not influence other results. Figure 9 shows that especially at higher temperatures the simulated Li-sites coincide with the actual ones. No dependency was found on whether a sulfur or halide atom is at the anion position

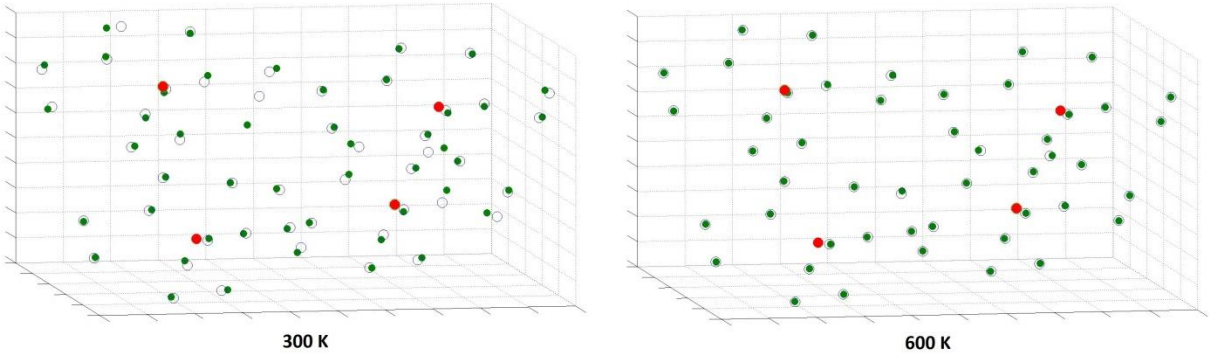

Figure 9 Lithium sites in Li_6PS_5Br. Variation between simulated lithium site (green dot) and actual crystallographic site (blue circle) decreases with higher temperature. No difference is visible between sulfur and halide atoms at the anion position Red dots indicate centers of cages.

Pathways in Li_6PS_5Br

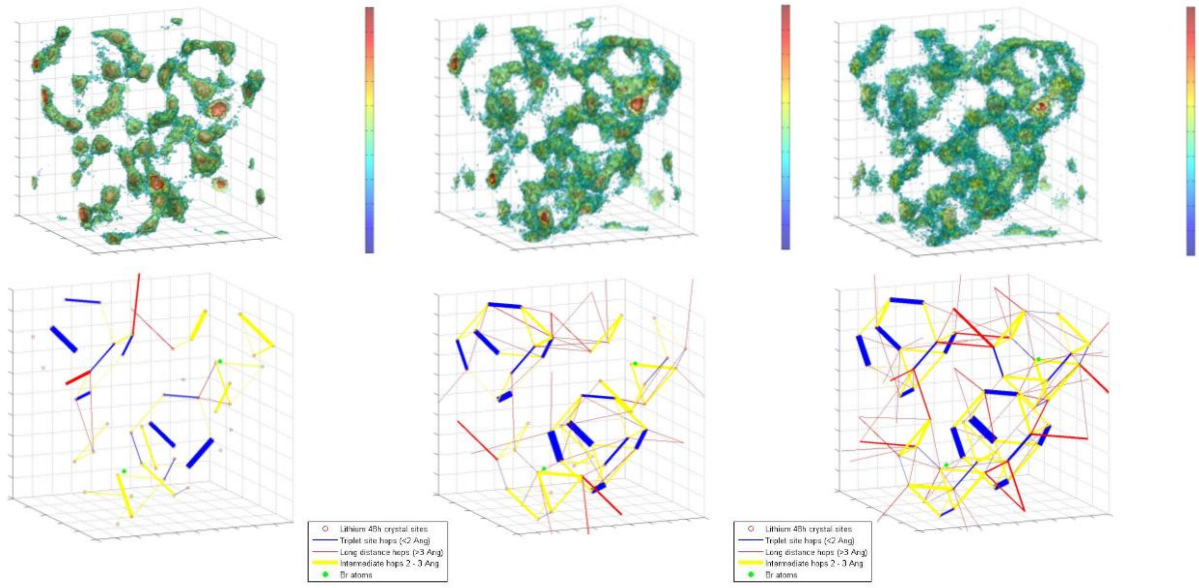

Figure 10 The Li-density and Li-jumps for Li6PS5Br at 300 K (left), 450 K (middle) and 600 K (right)

In Figure 10 Li-density maps and Li-jumps are shown. At low temperature (300 K) the density map does not show Li-pathways which run throughout the unit cell, but upon increasing the temperature interconnected pathways appear. As shown in Figure 10 there are 3 types of Li-jumps in Li_6PS_5Br, the thickness of the lines corresponds to the jump rate. At 600 K the mean jump rate per lithium equals $1.57 \cdot 10^{11}$ s^{-1}. The blue lines show jumps between 48h sites via 24g sites (1.68 Å apart), the yellow lines show jumps between the remaining connections of 48h sites within one 'cage' surrounding a sulphur or halide atom (2.48 Å), and the red lines show jumps between 48h sites in different 'cages' (>3 Å). The red jumps are the most important since these make pathways through the crystal. At 300 K there are some red jumps, so the Li-ions can move through the whole crystal, but the MD-simulations are too short to capture this in the density map. At higher temperatures more red lines appear, showing that the pathways become better connected, leading to increased macroscopic diffusion. The mean jump distance increases from 2.6 to 3 Angstrom between 300 K and 600 K.

The bromine atoms change the diffusion pathways in their surroundings, causing lithium to hop less often along the blue connections and more often along the yellow connections in Figure 10. This variation in environment has impact on the long range diffusivity of lithium. An alternating pattern of sulphur and bromine on the anion positions shows most red connections, promising best macroscopic diffusion.

Pathways in Li_6PS_5Cl

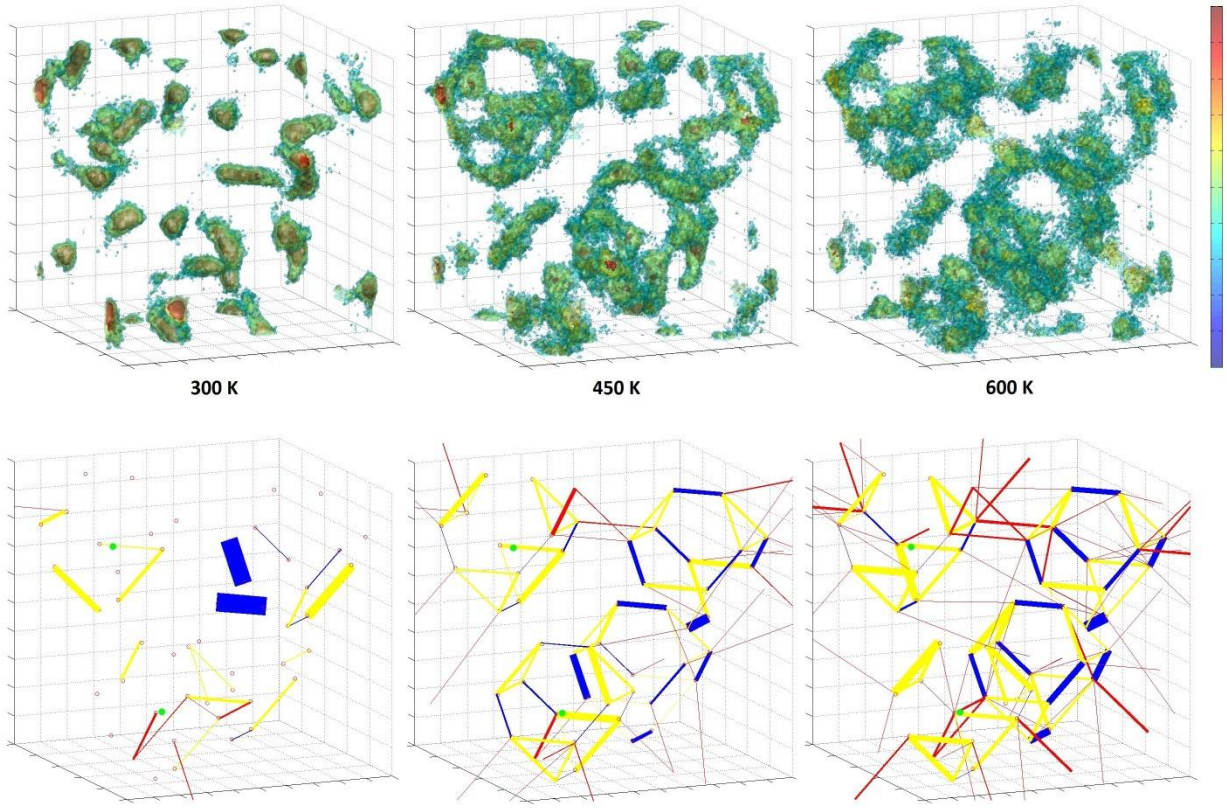

Figure 11 The Li-density and Li-jumps in Li_6PS_5Cl at 300 K (left), 450 K (middle) and 600 K (right).

As shown in Figure 11 the lithium pathways in Li_6PS_5Cl have many similarities to the ones in Li_6PS_5Br. The blue lines show jumps between 48h sites via 24g sites (1.83 Å apart), the yellow lines show jumps between the remaining connections of 48h sites within one 'cage' surrounding a sulfur or halide atom (2.36 Å), and the red lines show jumps between 48h sites in different 'cages' (over 2.8 Å). Already at 300 K red lines are visible, meaning the lithium can move through the entire crystal. Higher temperatures show increased diffusivity with thicker colored lines. Jump rates are exceptionally high in this material, at 600 K rates of $2.10 \cdot 10^{11}$ s^{-1}.

Next to a single unit cell a 2x1x1 supercell of Li_6PS_5Cl has been simulated. The results are very good comparable: MSD diffusivities equal respectively 0.93 and 0.83 S/cm, and jump rates are even more on one line with $2.10 \cdot 10^{11}$ s^{-1} and $2.07 \cdot 10^{11}$ s^{-1} respectively. This indicates that a single unit cell does not suffer much from boundary interactions during a simulation.

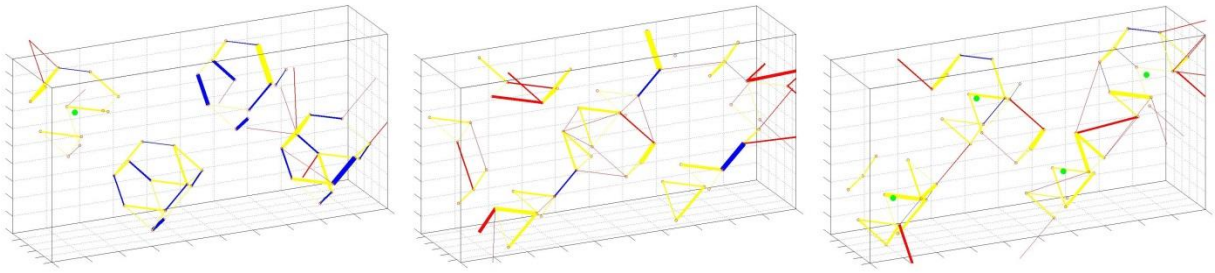

Figure 12 The Li-jumps in a 2x1x1 supercell of Li_6PS_5Cl at 450 Kelvin that is cut into three slices which are presented next to each other.

Figure 12 shows the diffusion pathways in three slices of a Li_6PS_5Cl 2x1x1 supercell at 450K. The middle of this cell has its sulfur and chloride atoms ordered plane like, while the left and right extremities of this cell have these atoms ordered alternatingly. More and thicker red connections are visible on the left and right sides than are in the middle of each slice, indicating that alternating ordering results in better lithium diffusivity. In the middle of the first slice in Figure 12 succeeding anion sites occupied by sulfur atoms show no red lines along that plane. Connections to parallel planes still allow for macroscopic diffusion past the succeeding sulfurs, although with a detour.

Pathways in Li_6PS_5I

The poor diffusivity of Li_6PS_5I compared to Li_6PS_5Br and Li_6PS_5Cl becomes immediately clear from the Li-pathway plots. At 300K there are only blue connections, in contrast to the other two halide compounds. Even at 600K there are no red connections, as visible in Figure 13.

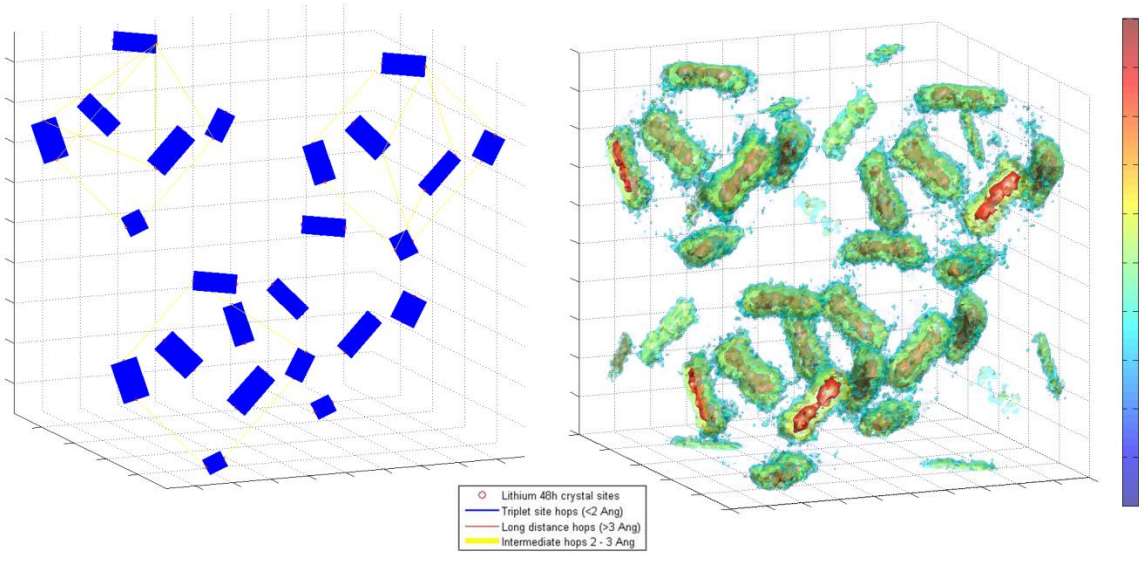

Figure 13 The Li-density and Li-jumps in Li_6PS_5I at 600 Kelvin.

The iodide in Li_6PS_5I is highly ordered outside the 'cages' in contrast to the other halide compounds, explaining the radical pathway difference. The doublet spots are squeezed tightly together (1.13 Å apart) compared to Li_6PS_5Cl (1.83 Å) and Li_6PS_5Br (1.68 Å), resulting in the two sites acting as one (Figure 14). Because the spacing almost equals the radius of a lithium atom, it prevents the two spots from being occupied simultaneously, limiting lithium mobility.

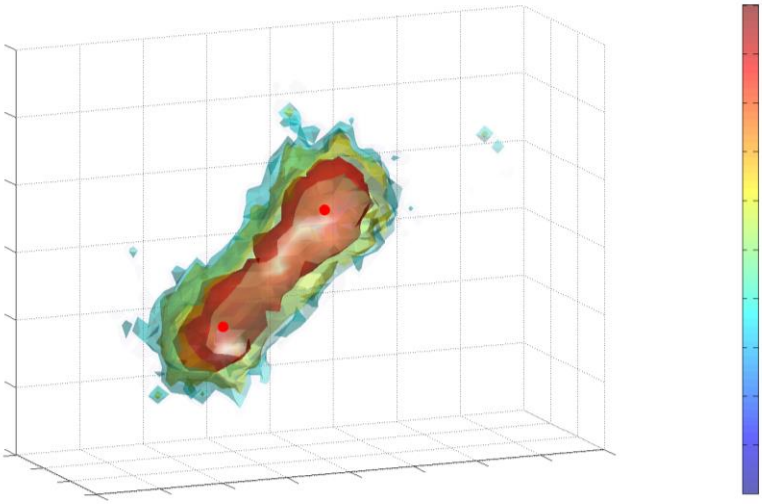

Figure 14 The Li-density on a doublet site in Li_6PS_5I at 600 Kelvin, showing behavior of a single site.

$Li_5PS_4Cl_2$ results

The positive effects of halide disorder over the anion sites are verified by simulations of the not yet synthesized $Li_5PS_4Cl_2$, which shows especially high diffusivities of 2 S/cm at 600 K. This material has all anion sites occupied by chlorine, by which means all 'cage' structures are benefitting from the halide influence. The Li-density maps and Li-pathways are shown in Figure 15.

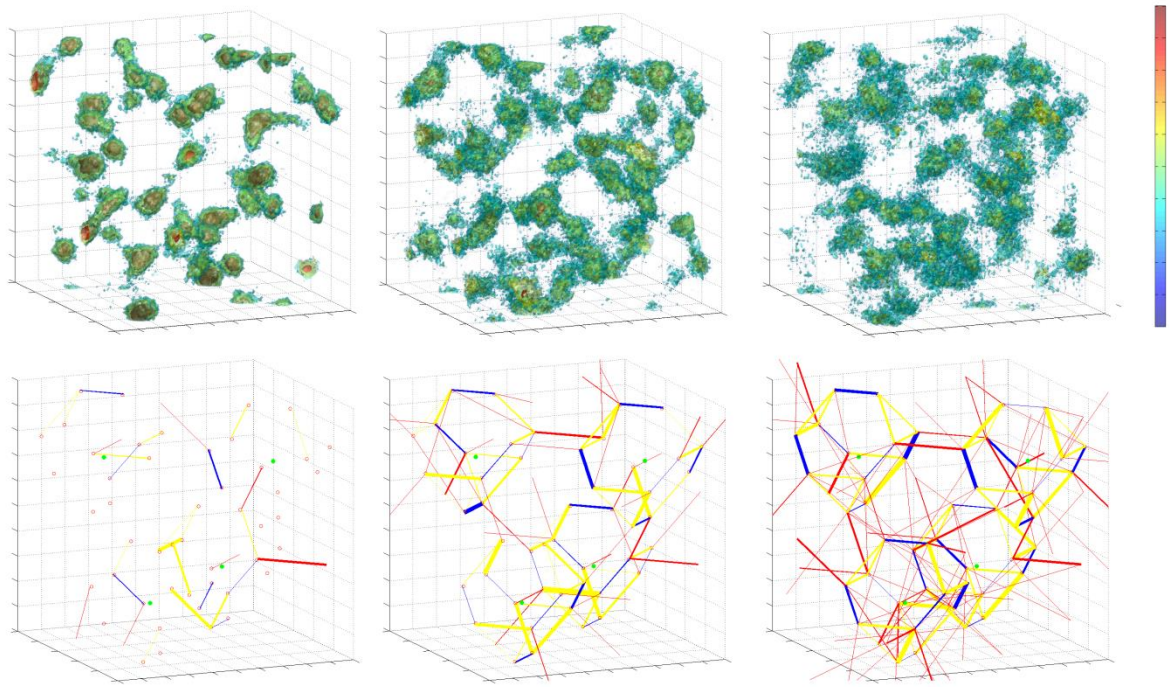

Figure 15 The Li-density and Li-jumps in $Li_5PS_4Cl_2$ at 300 K (left), 450 K (middle) and 600 K (right).

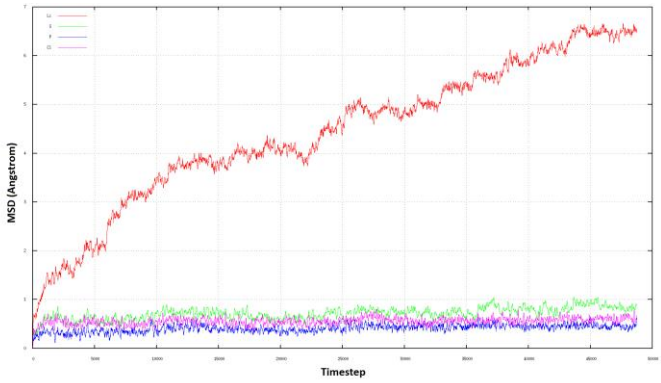

Figure 16 MSD's for all atoms in $Li_5PS_4Cl_2$ during a simulation at 600 K, showing that the crystal is stable and only lithium is moving.

Li_7PX_6 (X = S, Se) compounds results

The Li_7PX_6 (X = S, Se) have worse diffusivities than the Li_6PS_5X (X = Cl, Br), in line with the previously encountered positive effect of halide disorder on the anion sites. The pathways in both Li_7PX_6 materials are similar to the pathway cages around the sulfurs in Li_6PS_5Cl and Li_6PS_5Br. However, density plots show the lack of 24g interstitial sites, which could be explained by a major change in potential energy landscape.

Pathways in Li_7PS_6 and Li_7PSe_6

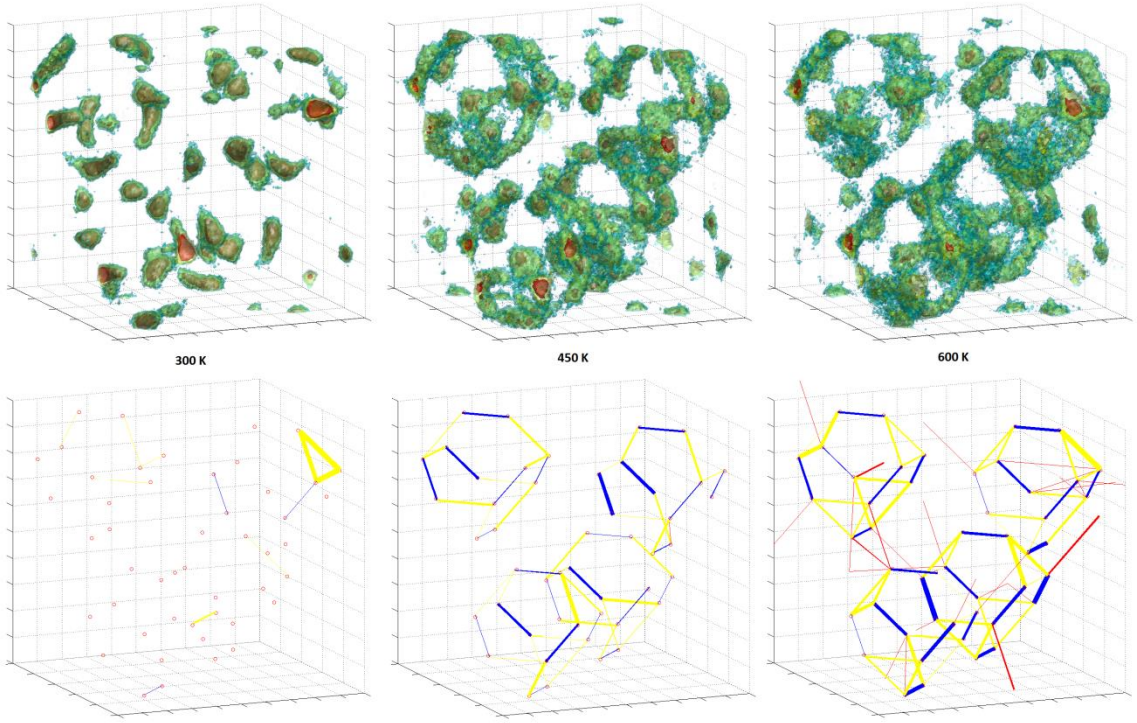

Figure 17 Lithium density plots for Li_7PS_6 at 300 K, 450 K and 600 K. The red zones (indicating the highest occupancy) are only at 48h positions.

Figure 17 shows the lithium pathways in Li_7PS_6. The blue lines show jumps between close 48h sites (1.90 Å apart), the yellow lines show jumps between the remaining connections of 48h sites within one 'cage' surrounding a sulfur or halide atom (2.25 Å), and the red lines show jumps between 48h sites in different 'cages' (over 2.80 Å). The same values apply to Li_7PSe_6, which pathways are shown in Figure 18. The jump rates in the materials are $8.45 \cdot 10^{10}$ s^{-1} in Li_7PS_6 and $1.4 \cdot 10^{11}$ s^{-1} in Li_7PSe_6. No differences are found between the pathways of Li_7PS_6 and Li_7PSe_6 that could explain the slightly better conduction in the latter.

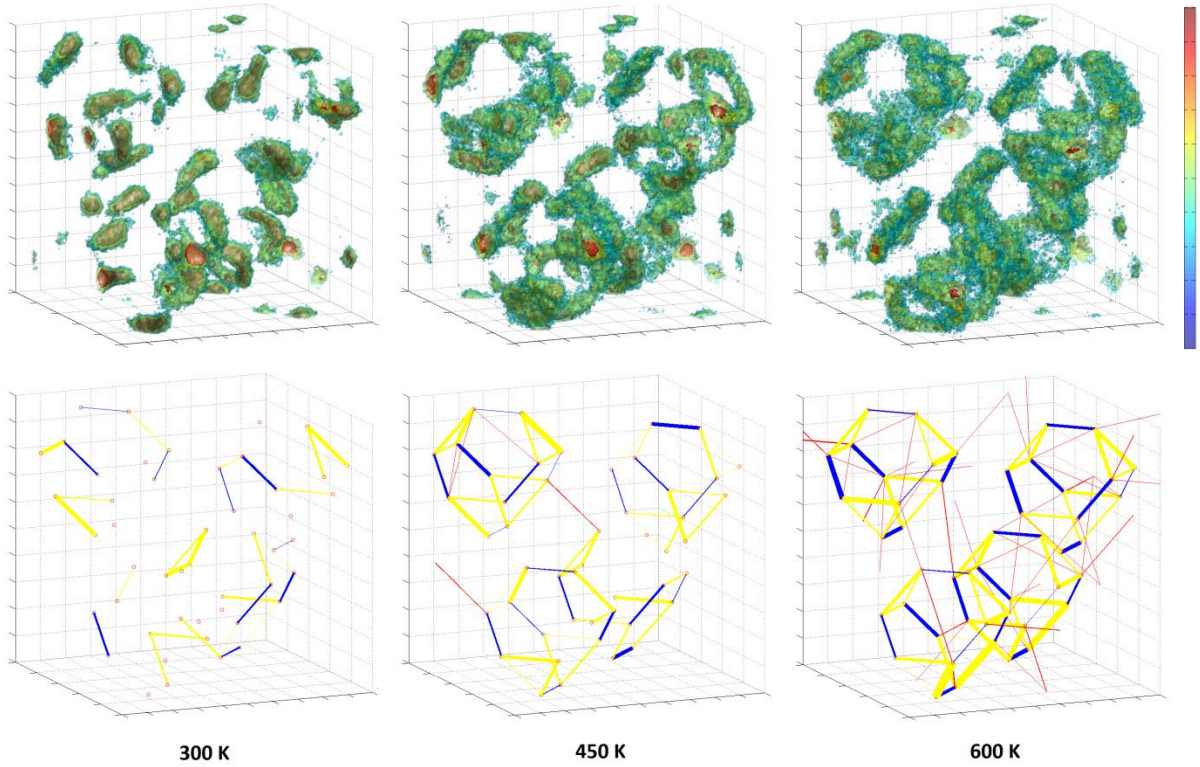

Figure 18 Lithium density plots for Li_7PSe_6 at 300 K, 450 K and 600 K. The graphs show stunning similarities with Li_7PS_6.

The lithium distribution in Li_7PX_6 (X = S, Se) is more localized than in Li_6PS_5X (X = Br, Cl). This is best visible in the density plots at 600 K, where lithium in Li_6PS_5Br and Li_6PS_5Cl is more scattered than in Li_7PX_6. Both Figure 17 and Figure 18 show multiple red high density spots at this elevated temperature, but only few are visible in Figure 10 and Figure 11 corresponding to Li_6PS_5X (X = Br, Cl).

Detailed short range diffusivity in Li_7PX_6 (X = S, Se)

Figure 19 compares the lithium distribution over two close 48h sites in Li_7PSe_6 with a triplet site in Li_6PS_5Br. Clearly, lithium in Li_7PSe_6 resides far less between the two 48h sites than it does in Li_6PS_5Br. The jumping activity however is 4 times higher in the Li_7PSe_6. This could be explained by assuming a square well shaped potential for Li_7PSe_6, and a sinusoidal shaped potential for Li_6PS_5Br with a higher energy barrier. The jump rate is dependent on the energy barrier and the distribution is dependent on the shape of the potential. Therefore the broader sinusoidal potential would explain the spread distribution of Li_6PS_5Br, while a square well would explain the localization in Li_7PSe_6.

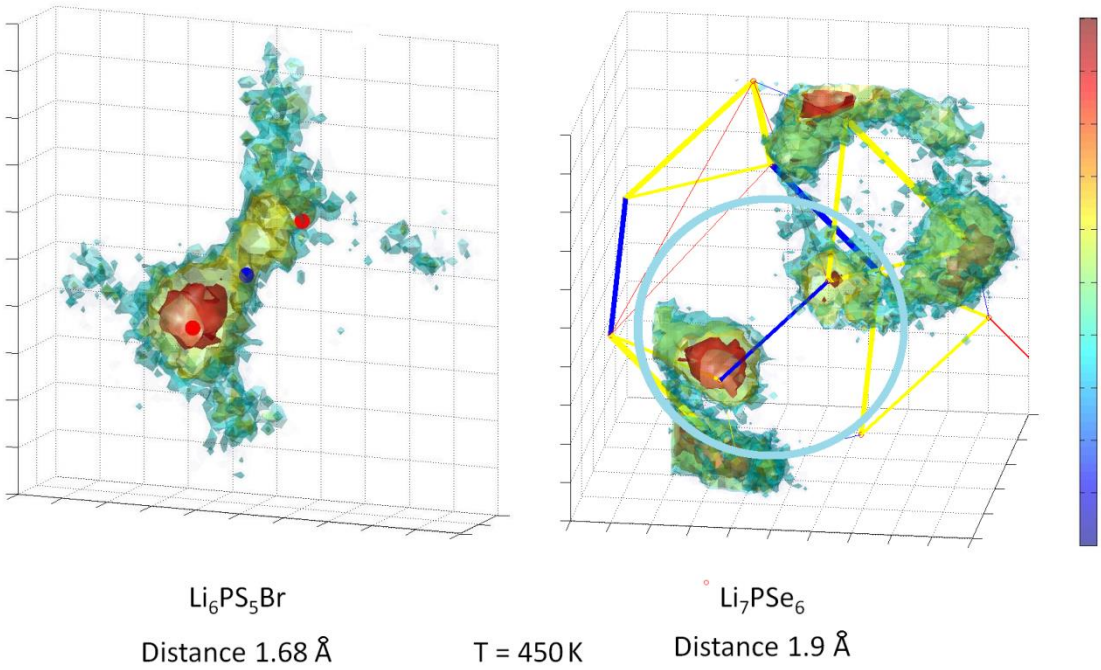

Figure 19 Comparison of a triplet site in Li_6PS_5Br with a doublet in Li_7PSe_6. The doublet has a far higher jump frequency between the two 48h sites than the triplet, while the density plot forms a bridge at the triplet site. A possible explanation is a square shaped potential at the doublet and a sinusoidal shaped potential at the triplet.

Effect of vacancies on Li-diffusivity

To investigate to effect of Li-vacancies on the diffusivity, Li_5PS_5Cl and Li_7PS_5Cl have been compared to the existing Li_6PS_5Cl. Only Li_6PS_5Cl is in fact an existing crystals, the other materials are created by adding or subtracting Li ions from the original structure. The Li_5PS_5Cl and Li_7PS_5Cl showed to be unstable at 600 K, therefore no conductivity results are listed in Figure 20 at this temperature.

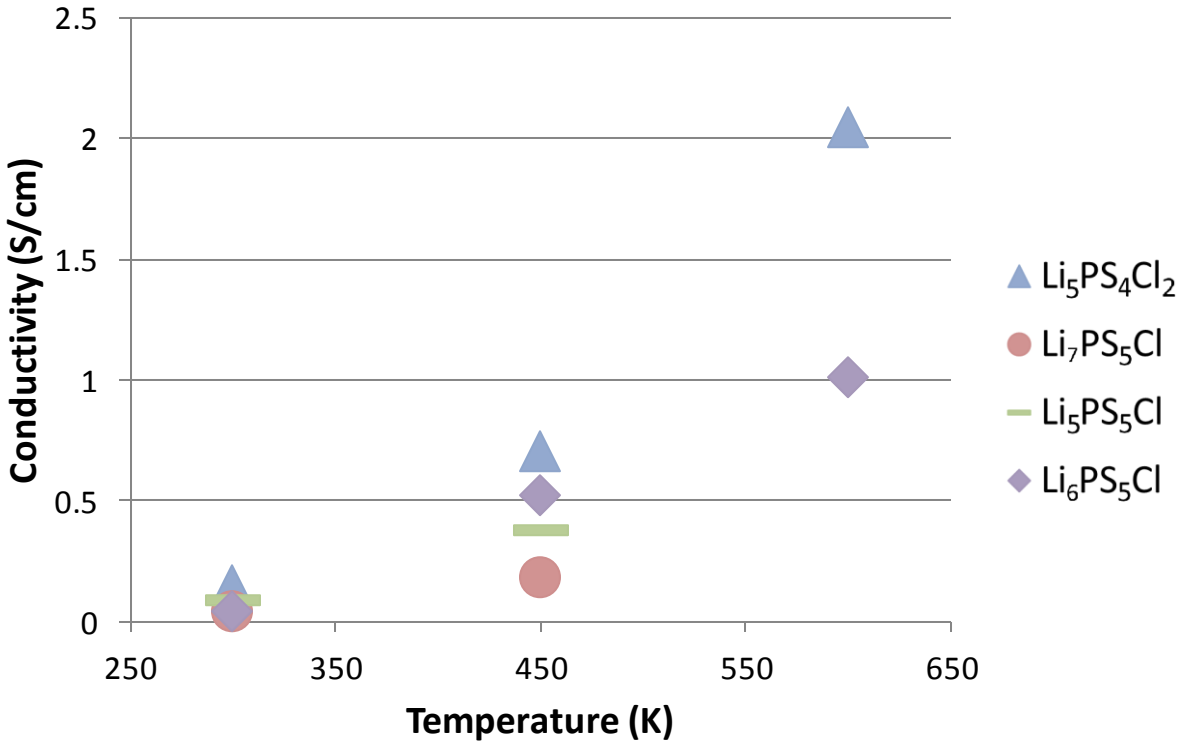

Figure 20 Conductivities in Li_nPS_5Cl (n = 5, 6, 7) and $Li_5PS_4Cl_2$ based on Li MSD's.

Figure 20 shows vacancies have a limited effect on Li diffusion, since both adding and subtracting lithium atoms reduces diffusivity. The $Li_5PS_4Cl_2$ compound, which has all anion sites occupied by chlorine, shows far better performance, indicating that the atomic environment has more influence on diffusivity than the vacancies. Comparison of Li_7PS_6 with Li_6PS_6 supports this conclusion. Figure 21 shows that also in this material vacancies have little influence on macroscopic diffusivity.

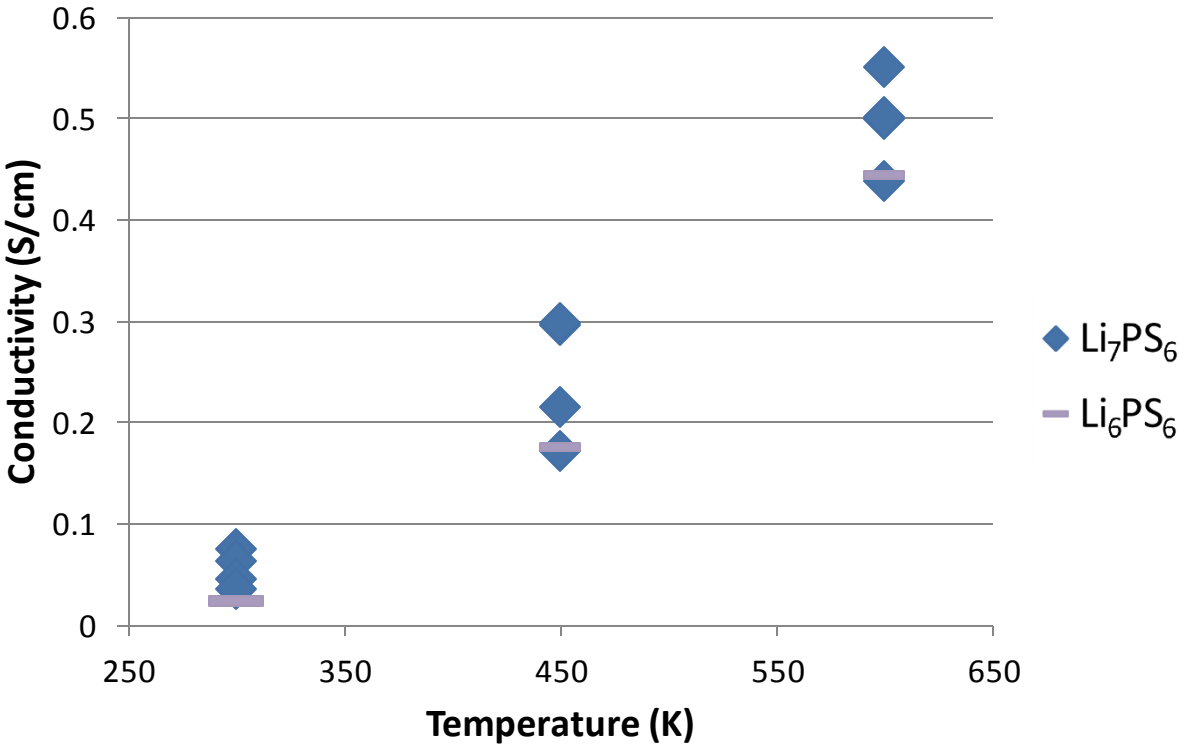

Figure 21 Conductivities in Li_nPS_6 (n = 6, 7) based on Li MSD's.

Jump rates

In Table 6 jump frequencies and average jump distances for relevant materials are listed. Column Ratio shows that conductivities based on jump frequencies differ significantly from MSD results at 300 K, but the values approach each other at higher temperatures. This indicates that at lower temperatures some Li atoms only exhibit local hopping, whilst at elevated temperatures all macroscopic pathways are being used.

Table 6 Jump rates, mean jump distances and conductivities from MD-simulations with 10 picoseconds equilibration time.

Structure	T (K)	Mean jump distance (Å)	Jump rate (s^{-1})	Jump rate conductivity (S/cm)	Ratio	MSD ($Å^2$)	MSD Conductivity (S/cm)
Li_7PS_6	300	2.3	$1.43 \cdot 10^{9}$	$1.84 \cdot 10^{-2}$	1	1.3	$3.20 \cdot 10^{-2}$
Li_7PS_6	450	2.3	$3.45 \cdot 10^{10}$	0.303	2	8.5	0.14
Li_7PS_6	600	2.4	$8.45 \cdot 10^{10}$	0.602	2	28.2	0.35
Li_7PSe_6	300	2.3	$2.82 \cdot 10^{10}$	0.367	6	2.4	0.06
Li_7PSe_6	450	2.3	$6.55 \cdot 10^{10}$	0.573	5	6.7	0.12
Li_7PSe_6	600	2.4	$1.40 \cdot 10^{11}$	1.00	1	48.7	0.67
Li_6PS_5Cl	300	2.5	$3.70 \cdot 10^{10}$	0.573	27	0.9	0.02
Li_6PS_5Cl	450	2.5	$1.17 \cdot 10^{11}$	1.21	2	30.3	0.50
Li_6PS_5Cl	600	2.8	$2.10 \cdot 10^{11}$	2.04	2	74.9	0.93
Li_6PS_5Cl (sc)	300	2.5	$4.14 \cdot 10^{10}$	0.638	14	1.7	0.05
Li_6PS_5Cl (sc)	450	2.5	$9.35 \cdot 10^{10}$	0.974	4	14.6	0.27
Li_6PS_5Cl (sc)	600	2.8	$2.07 \cdot 10^{11}$	2.02	2	60.0	0.83
Li_6PS_5Br	300	2.6	$4.44 \cdot 10^{10}$	0.728	5	5.9	0.16
Li_6PS_5Br	450	2.9	$9.95 \cdot 10^{10}$	1.39	4	21.0	0.39
Li_6PS_5Br	600	3	$1.57 \cdot 10^{11}$	1.78	2	60.0	0.83
$Li_5PS_4Cl_2$	300	2.4	$2.67 \cdot 10^{10}$	0.366	4	4.2	0.1
$Li_5PS_4Cl_2$	450	2.6	$1.24 \cdot 10^{11}$	2.38	3	43.0	0.711
$Li_5PS_4Cl_2$	600	3.1	$2.14 \cdot 10^{11}$	2.55	1	157.0	1.94

The 24g sites that would make up to the triplet sites are omitted in the jump rate calculations and pathway graphs in the next sections, because they are primarily used by the lithium as a passageway between 48h sites instead of really stationary crystal

sites. During a simulation the lithium atom moves very often up and back between these positions. The average residence time on a 24g site is 50 femtoseconds, while it is at least 100 femtoseconds on a 48h site and often much longer. Evidently the lithium only passes through the 24g spot rather than staying there.

Conclusion

Diffusivity values and lithium distributions in Li_6PS_5X (X = Cl, Br, I) and Li_7PX_6 (X = S, Se) are investigated using MD simulations. The best lithium conduction is found in Li_6PS_5Cl with diffusivity over 1 S/cm at 600 K. The change of lithium pathways near halide atoms plays a prominent role in lithium diffusion. Disorder of chlorine and bromine on anion sites opens pathways in the neighborhood enabling higher conductivities. Strictly ordered iodide in Li_6PS_5I shows unfavorable influence blocking lithium pathways leading to a lower conductivity of 0.08 S/cm at 600 K. For materials with partial halide disorder on the anion sites an alternating pattern is most favorable for high lithium diffusion.

The halide rich $Li_5PS_4Cl_2$ shows promising results with diffusivity of over 2 S/cm at 600 K, clearly benefitting from having all its anion sites occupied by chlorine. Comparative study of Li_nPS_5Cl (n = 5, 6, 7) and Li_nPS_6 (n = 6, 7) shows no significant influence of lithium vacancies on the diffusivity of lithium in these materials.

Both Li_7PS_6 and Li_7PSe_6 show a more localized lithium distribution compared to the Li_6PS_5X (X = Cl, Br, I) group. However, this does not hinder lithium diffusivity. The lithium pathways have been categorized into three groups, depending on the corresponding jump distances and morphology. Jump rates in both material families are in the order of 10^{10} s^{-1}, while Li_6PS_5Cl and $Li_5PS_4Cl_2$ show the highest jump rates of respectively $2.10 \cdot 10^{11}$ s^{-1} and $2.14 \cdot 10^{11}$ s^{-1} at 600 K.

Recommendations

Based on the MD results the best Li-conductor in the Li_6PS_5X (X = Cl, Br, I) and Li_7PX_6 (X = S, Se) families is Li_6PS_5Cl. Real life performance of Li_6PS_5Cl and Li_6PS_5Br can be improved by ensuring that the halide disorder follows an alternating pattern. Furthermore, ways to achieve higher anion disorder ratios during the synthetization process should be sought in order to increase lithium diffusivity in these materials.

Possibilities of synthesizing the promising $Li_5PS_4Cl_2$ are to be evaluated, since this material performs better in the simulations than the existing families mentioned above. The simulations show that this material is stable, insulating and a particularly good lithium conductor. Therefore this material would be a good runner up for a solid state electrolyte.

In future MD simulations a broader use of higher level languages for data analysis purposes is recommended. While the VASP routines are reasonably written in a low level language allowing for faster execution (Fortran), the analysis tools do not necessarily have to be written this way. Higher level environments (Matlab, Python) are more versatile and easier to debug at the exchange of performance. Efficient integration of both environments requires optimization of the output files from VASP for easier loading to the higher level environments, since this turned out to be a bottle neck during the analysis in this report.

Follow up studies of the MD simulations could also take into account the potentials of different atoms, especially during jump events. This allows for a deeper understanding of the diffusion mechanisms and processes occurring.

Acknowledgments

First I want to thank both N. de Klerk and dr. ir. M. Wagemaker for their help and guidance in writing this bachelor thesis. Furthermore I would like to thank both Chuang Yu and Swapna Ganapathy for answering my questions and helping me when I was in doubt. And also all the others from the staff of FAME with who I spend a good time at the Reactor Institute in Delft writing this thesis.

References

1. *Recent progress in high-voltage lithium ion batteries.* **Hu, M., Pang, X. and Zhou, Z.** s.l. : Journal of Power Sources, 2013.

2. *How Electrolytes influence battery safety.* **Roth, E.P. and Orendorff, C.J.** s.l. : The Electrochemical Society, 2012.

3. *Li6PS5X: A class of crystalline Li-Rich Solids With an Unusaually High Li+ Mobility.* **Deiseroth, H.-J., et al., et al.** Weinheim : Angewandte Chemie, 2007.

4. *Li7PS6 and Li6PS5X (X: Cl, Br, I): Possible Three-dimensional DIffusion Pathways for Lithium Ions and Temperature Dependance of the Ionic Conductivity by Impedance Measurements.* **Deiseroth, H.-J., et al., et al.** Weinheim : Wiley-VCH, 2011.

5. **Hook, J.R. and Hall, H.E.** *Solid State Physics.* Salisbury : APS, 1991.

6. *DFT in a nutshell.* **Burke, Kieron and Wagner, L.O.** s.l. : International Journal of Quatnum Chemistry, 2012.

7. **Kohanoff, Jorge.** *Electronic Structure Calculations for Solids and Molecules.* Cambridge : Cambridge University Press, 2006.

8. **Mehrer, H.** *Diffusion in Solids: Fundamentals, Methods, Materials, Diffusion-Controlled Processes.* s.l. : Springer Science & Business Media, 2007.

9. **Wolfson, R.** *Essential University Physics.* Harlow : Addison-Wesley, 2007.

10. *On the theory of Brownian motion.* **Uhlenbeck, G.E. and Ornstein, L.S.** 35(5):823, s.l. : Physical review, 1930.

11. **Kresse, G. and Hafner, J.** 47, 558, s.l. : Physical Review B, 1993.

12. *Synthesis and Characterization of Lithium Argyrodite, Li7PS6.* **Kong, S.T., Reiner, C. and Deiseroth, H.J.** s.l. : WILEY-VCH Verlag, 2006.

13. *Variation in structure and Li+-ion migration in argyrodite-type Li6PS5X (X = Cl, Br, I) solid electrolytes.* **Rayavarapu, P.R., et al., et al.** s.l. : Springler-Verlag, 2011.